J Electroceram (2009) 22:180–184
DOI 10.1007/s10832-007-9363-4

# Micromachined piezoelectric structures for high-temperature sensors

**Jan Sauerwald · Michal Schulz · Denny Richter · Holger Fritze**

Received: 14 March 2007 / Accepted: 9 November 2007 / Published online: 29 November 2007


**Abstract** The availability of large size langasite ($La_3Ga_5SiO_{14}$) wafers enables micromachining of this high-temperature stable piezoelectric material which has been shown to exhibit bulk oscillations at temperatures of up to at least 1400 °C. In particular, the realization of miniaturized resonant sensors becomes feasible. Such resonators are operated far above their dielectric relaxation frequency leading to relatively low losses. Our specific research is focused on the development of monolithic structures to overcome problems originating from thermal stress. The concept includes the local doping of langasite by niobium, strontium and praseodymium. Their chemical diffusion coefficients were determined and found to be fairly small. Field enhanced diffusion results in an increased doping depth and concentration as demonstrated for niobium. The effect is governed by local heating of the sample. Optimized process conditions lead potentially to a pronounced drift of the dopants. Strontium doping increases the conductivity of langasite by three to four orders in magnitude and enables the formation of monolithic electrodes for high-temperature resonators as demonstrated by operation of such devices at temperatures as high as 800 °C. Micromachined functional structures including planar and biconvex membranes, as well as cantilevers, are prepared and demonstrated to be operational up to 930 °C. The analysis of their resonance behavior shows high resonator quality factors, e.g. 190 for a 60 MHz bulk acoustic resonator at the above-mentioned temperature.

J. Sauerwald · M. Schulz · D. Richter · H. Fritze (✉)
Faculty of Natural and Materials Sciences,
Technical University of Clausthal,
Clausthal-Zellerfeld, Germany
e-mail: holger.fritze@tu-clausthal.de

**Keywords** Langasite · MEMS · Piezoelectricity · Gas sensor · High temperature

## 1 Introduction

Quartz resonators vibrating in the thickness-shear mode are well known as quartz crystal microbalances. Very small mass changes during film deposition onto resonators or gas composition dependent stoichiometry changes of thin films already deposited onto the resonators can be correlated with their resonance frequency shift. The operation of such piezoelectric transducers can be extended to temperatures above the operation limit of quartz (~500 °C) by applying materials that retain their piezoelectric properties up to higher temperatures. In particular, langasite ($La_3Ga_5SiO_{14}$) enables operation temperatures up to at least 1000 °C [1]. The ultimate temperature limit is close to its melting point at 1470 °C [2].

The availability of high quality and large size langasite wafers [3, 4] enables micromachining of this material. Well known advantages of this technique such as miniaturization and cost-effective production can be used to create high-temperature stable piezoelectric structures. Crucial issues in designing such miniaturized structures include excessive mechanical and electrical losses as well as thermal stress.

Losses might be lowered by:

(1) Modification of the piezoelectric material by e.g. doping and
(2) Appropriate choice of the resonance frequency.

Issue (1) is not subject of this paper since it is already discussed in [5, 6]. Issue (2) can be realized preferably by miniaturization. Losses related to the static resistance $R_S$ (or

conductance $G_S$) of the extended Butterworth-van Dyke equivalent electrical circuit [7] shift the entire resonance curve $G(f)$. Consequently, the sharpness of the resonance peak remains unchanged as visualized in Fig. 1. In contrast, the mechanical loss expressed as $R_M$ (or $G_M$) impacts the accuracy in frequency determination. High values cause shallow peaks. A detailed analysis of the resonance behavior based on a one-dimensional physical model [6] points to a loss maximum at the (angular) dielectric relaxation frequency $\omega_\varepsilon = 2\pi f_\varepsilon = \sigma_R/\varepsilon_R$ [8]. The contribution, denoted by $R_\sigma$ in Fig. 2, decreases with increasing operation frequency. Consequently, resonator operation at high frequencies is recommended. Micromachining provides appropriate tools to create such resonators.

In order to overcome problems originating from thermal stress between e.g. the piezoelectric material and the electrodes special emphasizes is taken on the development of monolithic structures. The concept includes the local doping of langasite by niobium, strontium and praseodymium since it is expected to result in locally increased conductivities to form electrodes. Section 2 presents the kinetics of doping and options to increase the doping depth. Another anticipated effect of doping is the modification of the rate of wet chemical etching and, thereby, the option to etch the material locally. The issue is addressed in a minor way in Section 3. Finally, the operation of miniaturized structures is tested at elevated temperatures and presented in Section 4.

## 2 Doping of langasite

### 2.1 Chemical diffusion

Langasite can be doped by a variety of cations. The sites where they substitute into are known [9–12]. Based on the ionic radii and the coordination numbers strontium or praseodymium dopants occupy $La^{3+}$ sites. Under these circumstances, strontium acts as an acceptor whereas praseodymium is a neutral substituent or a donor. Niobium replaces $Ga^{3+}$ thereby acting as a donor.

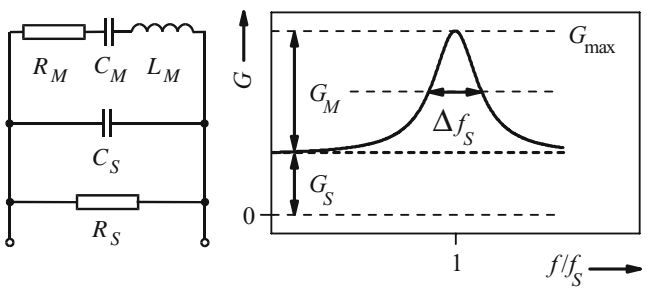


**Fig. 1** Extended Butterworth-van Dyke equivalent electrical circuit (*left*) and conductance spectra (*right*) for bulk acoustic resonators operated at elevated temperatures

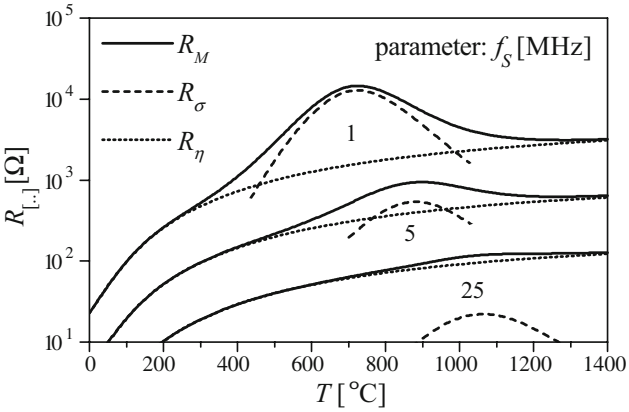


**Fig. 2** Temperature dependent values of $R_M$, $R_\sigma$ and $R_\eta$ calculated for 1, 5 and 25 MHz langasite resonators

The chemical diffusion of these dopants is investigated by deposition of thin film tracer sources, thermal diffusion and subsequent secondary ion mass spectrometry. Since *y*-cut resonators are of interest, the transport along the *y*-axis is examined. The diffusion coefficients of strontium, praseodymium, and niobium are fairly small as shown in Fig. 3. Their temperature dependence can be described by $D=D_0 \exp(-E_A / kT)$. The parameters of niobium are $D_0=2.9\times10^{-12}$ m$^2$/s and $E_A=1.8$ eV. Strontium and praseodymium exhibit virtually the same diffusivity which is consistent with their similar ionic radii and the occupation of the same site in the langasite lattice. For both elements $D_0=1.1\times10^{-4}$ m$^2$/s and $E_A=4.5$ eV is found.

The characteristic diffusion depth $y_{diff}$ can be estimated from the diffusion coefficient $D$ and the annealing time $t$ according to $y_{diff}=2(Dt)^{1/2}$. At 1400 °C, where the diffusion coefficients of strontium, praseodymium and

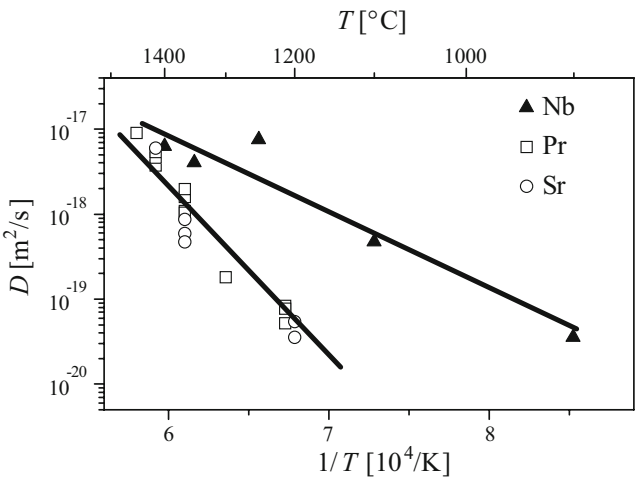


**Fig. 3** Arrhenius plot of the diffusion coefficients of niobium, strontium and praseodymium along the *y*-direction in langasite single crystals

niobium are quite similar, a diffusion depth of 5 μm requires annealing periods of several days. Consequently, the preparation of locally doped langasite samples by thermal diffusion might be time consuming and prevent the application of the method. Contrary, once the doping is performed, operation temperatures of 900 °C virtually do not change the extent of the doped region. For example, $y_{diff}$ increases for strontium or praseodymium from 3.0 to 3.1 μm within 4,000 years.

### 2.2 Field enhanced diffusion

Electrical field enhanced diffusion is performed in order to increase the doping depth and concentration. After deposition of a niobium source layer on one side of a langasite sample, both sides of the sample are partially coated by platinum electrodes to enable the application of a voltage. The approach minimizes errors (source layer thickness, thermal treatment etc.) since niobium's depth profiles created with and without field enhancement can be taken from the same sample.

During the thermal treatment ($T_D$=1000 °C, $t_D$=24 h) an electrical field ($E$≈90 kV/m) is applied ($t_E$=1 h). Thereby, the electrical current leads to local heating of the sample as it becomes obvious by changes of the sample resistance. In order to avoid damage of the sample, the temperature is kept constant ($T_E$=1160 °C) using the resistance for the control process. The application of the electrical field results in an increased doping depth and concentration as shown in Fig. 4. The fact is highly important from a practical standpoint. Two effects are presumably responsible:

(1) Drift of the niobium ions induced by the electric field and
(2) Local heating of the sample which increases the diffusivity and the exchange of niobium at the langasite surface.

If the drift is considered solely, the penetration depth can be calculated by $y_{drift} = E\ \mu\ t$. Introducing the Einstein relation to replace the mobility $\mu$, $y_{drift} = Eq\ D\ t/kT$ follows. Here, $q$ and $k$ are the effective charge of niobium (assumed to be $q = e$) and the Boltzmann constant. For the experimental conditions chosen here ($T_E$=1160 °C, $t_E$= 1 h, $D$=1.3×10$^{-18}$ m$^2$/s) the penetration depth increases by about 3 nm. On the contrary, the change of the diffusion coefficient due to the local heating causes an increase in penetration depth by about 87 nm. The value follows from the difference of $y_{diff}$ for the experimental conditions with ($T_E$=1160 °C, $t_E$=1 h) and without ($T_D$=1000 °C, $t_E$=1 h) electrical field. Fig. 4 shows an increase in penetration depth of up to about 100 nm. Consequently, the field enhancement plays a minor role.

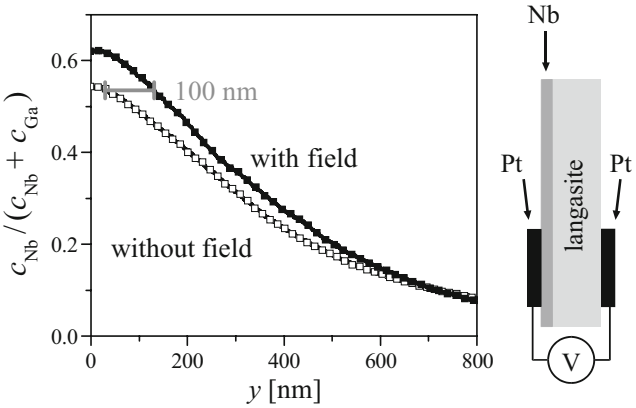


**Fig. 4** Depth profile of niobium after diffusion without and with application of an external electrical field (*left*) and sample geometry (*right*)

The diffusion and drift related penetration depth is a square root and a linear function of time, respectively. Therefore, drift terms might dominate at prolonged times. The transition time $t_T$ follows from $y_{Diff} = y_{Drift}$ which results in $t_T = 1/D\ (2kT/Eq)^2$. For the experimental conditions chosen so far ($T_E$=1160 °C, $D$=1.3×10$^{-18}$ m$^2$/s, $E$= 90 kV/m) a transition time of about 67 days follows. The value must be reduced dramatically in order to make the field enhancement usable. A process temperature close to the melting point ($T_E$=1450 °C, $D$=1.2×10$^{-17}$ m$^2$/s) and a higher field strength ($E$=300 kV/m) result in a transition time of less than one day. It remains to be proven if such experimental conditions are feasible. One critical issue is the temperature control based on the sample resistance.

### 2.3 Highly conductive areas

The anticipated effect of strontium on the conductivity is verified by locally doped areas which are prepared by

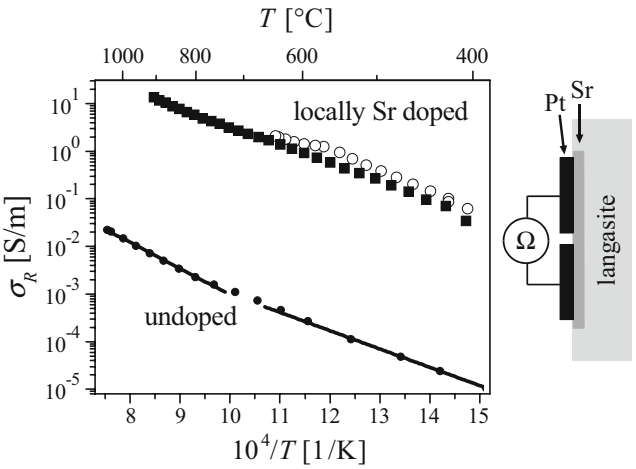


**Fig. 5** Conductivity of nominally undoped langasite and of a strontium doped layer

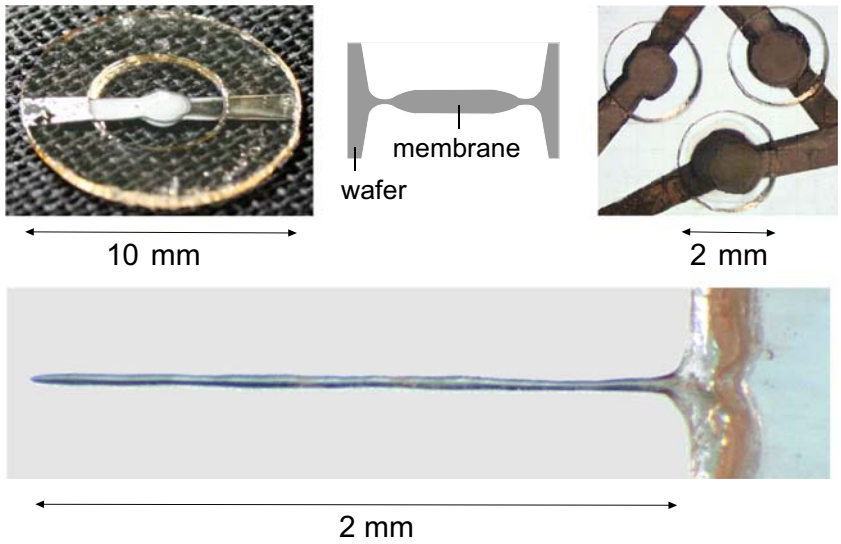


**Fig. 6** Examples for etched langasite structures: Biconvex membrane (including schematic cross section), membrane array and cantilever beam (thickness about 30 μm)

inward diffusion of this element. The langasite samples evaluated here exhibit a strontium concentration of up to $6\times10^{21}$ $cm^{-3}$ in an effectively 2.7 μm thick surface layer. About 60% of lanthanum is expected to be replaced by strontium, which is in agreement with the option to replace lanthanum largely [9]. The conductivity prediction according to the defect model for langasite [13] points to an increase in conductivity by some orders in magnitude if the material is highly acceptor doped. The expectation corresponds to the experimentally determined change in conductivity of the locally doped area by three to four orders in magnitude as shown in Fig. 5. The statement results from impedance measurements with subsequent calculations of the conductivity by finite element methods to account for the sample geometry.

The result confirms the effect of strontium doping predicted by the defect model. However, quantitative comparisons should not be given since the extrapolation of the conductivity prediction to high dopant levels as well as the determination of the conductivity of the doped area is a rough estimation, only. The usability of the effect is demonstrated in Section 4 where strontium doped areas are used as electrodes.

## 3 Preparation of micro-electromechanical structures

In order to demonstrate the etching process and the potential of langasite as substrate for bulk micro-machining, micro-cantilever beams and membranes are designed and structured. Details can be found in [2, 14]. Essentially, langasite can be etched by $H_3PO_4$ showing etch rates of up to 90 μm/h at process temperatures above 100 °C.

Figure 6 shows examples for etched langasite structures which are a biconvex membrane, a membrane array and a cantilever beam. Thickness and length of the latter are about 30 μm and 2 mm, respectively. It should be mentioned that biconvex membranes are produced in two ways:

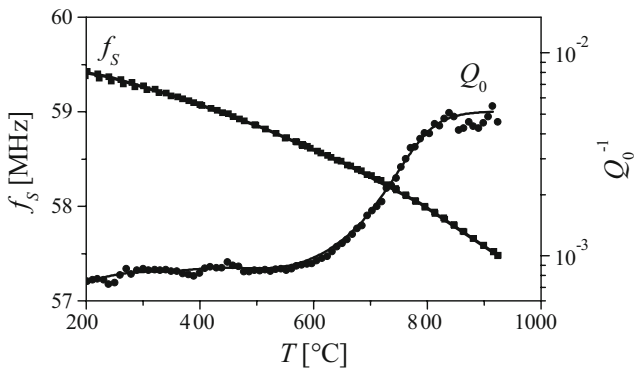


**Fig. 7** Temperature dependent resonance frequency and resonator quality factor of an about 23 μm thick langasite membrane

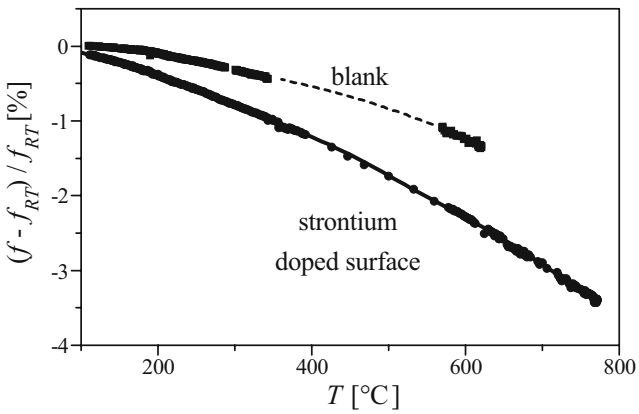


**Fig. 8** Temperature dependent resonance frequency of a langasite resonator with strontium doped areas used as electrodes

(1) Conventional etching in two steps with different masks and
(2) Preferential etching of a praseodymium doped area.

The second way takes advantage of an increased etch rate of praseodymium doped langasite areas by a factor of 40. The membranes are prepared by initial doping of ring-shaped areas on both sides of the sample and subsequent etching.

Further, the increased conductivity of strontium doped areas is used to create monolithic electrodes. They are prepared by thermal diffusion after local deposition of strontium carbonate. For reference, a resonator blank without such electrodes is prepared.

## 4 Test of miniaturized langasite structures

The temperature dependent resonance frequency and resonator quality factor of an about 23 μm thick planar langasite membrane are given in Fig. 7. Most remarkably, the 60 MHz membrane shows resonances up to about 930 °C.

The resonator quality factor $Q_0$ presented here follows from the resonance frequency $f_S$ and the bandwidth $\Delta f_S$ according to $Q_0 = f_S/\Delta f_S$. The bandwidth is determined at half maximum of the conductance $G_M$ squared. $Q_0$ reflects solely mechanical losses. In other words, the loss contribution related to $G_S$ is ignored since it does not decrease the accuracy in frequency determination [6]. The observed $Q$-factors of 60 MHz resonators are relatively high, i.e. about 620 and 190 at 700 and 930 °C, respectively (see Fig. 7). Further increase of the $Q$-factor is realized by biconvex membranes using the effect of improved energy trapping. A 16 MHz membrane exhibits a $Q$-factor of 770 at 700 °C (not shown). Due to the high resonance frequency, such membranes are operated far above their dielectric relaxation frequency leading to low contributions of $R_\sigma$ to the mechanical losses thereby lowering the total loss.

The $Q$-factors must be seen in the context of high temperature operation of the resonators. Conventional sized, i.e. planar 5 MHz resonators, show a value of about 460 at 700 °C, only. Extremely high values as reported for room temperature operation of e.g. quartz resonators can not be expected.

Figure 8 shows the resonance frequency of a resonator with monolithic electrodes, i.e. strontium doped langasite areas, as a function of temperature. The resonator exhibits strong resonances up to 800 °C which confirms the concept of monolithic electrodes. For reference, a resonator blank without electrodes is presented in the same plot. However, its signal is very weak and not suited for sensing purposes.

## 5 Conclusions

The diffusion coefficients of strontium, praseodymium, and niobium are fairly small. Consequently, the preparation of locally doped langasite samples by thermal diffusion might be time consuming and prevent the application of the method. Field enhanced diffusion is demonstrated to increase the penetration depth and concentration of dopants. The effect is governed by local heating of the sample. However, optimized process conditions may lead to a pronounced drift of the dopants.

Local strontium doping of langasite increases the conductivity by three to four orders in magnitude. Those areas are suited to serve as monolithic electrodes.

Langasite structures are machined by wet chemical etching. For example, thin bulk acoustic wave resonators can be used at temperatures as high as 930 °C. They show relatively losses since they are operated far above the dielectric relaxation frequency of langasite,

**Acknowledgements** The authors thank Dr. S. Ganschow from Institute of Crystal Growth, Berlin-Adlershof, Germany, for providing the langasite crystals. In addition, the fruitful collaboration with Prof. H. L. Tuller and Dr. H. Seh from Massachusetts Institute of Technology is acknowledged. Financial support from German Research Foundation (DFG) made this work possible.

## References

1. H. Fritze, M. Schulz, H. Seh, H.L. Tuller, Mater. Res. Soc. Symp. Proc **835**, 157 (2005)
2. J. Sauerwald, H. Fritze, E. Ansorge, S. Schimpf, S. Hirsch, B. Schmidt, International Work-shop on Integrated Electroceramic Functional Structures, Berchtesgaden, Germany, June 6–8, 2005
3. K. Shimamura, H. Takeda, T. Kohno, T. Fukuda, J. Cryst. Growth **163**, 388 (1996)
4. B. Chai, J.L. Lefaucheur, Y.Y. Ji, H. Qiu, Proceedings of the 1998 IEEE International Frequency Control Symposium, p. 748–760 (1998)
5. H. Fritze, M. Schulz, H. Seh, H.L. Tuller, Solid State Ionics **177**, 2313 (2006)
6. H. Fritze, Habilitation Thesis, TU Clausthal (submitted)
7. K. S. van Dyke, Proc. IRE, **16** 742 (1928)
8. T. Ikeda, *Fundamentals of piezoelectricity.* (Oxford University Press, Oxford, 1990)
9. B. V. Mill, Y. V. Pisarevsky, Proceedings of the 2000 IEEE/EIA International Frequency Control Symposium and Exhibition, p. 133–144 (2000)
10. A.A. Kaminskii, B.V. Mill, G.G. Khodzhabagyan, A.F. Konstantinova, A.I. Okorochkov, I.M. Silvestrova, Phys. Stat. Sol. (A) **80**, 387 (1983)
11. I.H. Jung, Y.H. Kang, K. Joo, A. Yoshikawa, T. Fukuda, K.H. Auh, Mater. Lett **51**, 129 (2001)
12. B.H.T. Chai, A.N.P. Bustamante, M.C. Chou, Proceedings of the 2000 IEEE/EIA International Frequency Control Symposium and Exhibition, p. 163–168 (2000)
13. H. Seh, Ph. D. Thesis, MIT (2005)
14. E. Ansorge, S. Schimpf, S. Hirsch, J. Sauerwald, H. Fritze, B. Schmidt, Sens. Actuators, A **132**, 271 (2006)